JGR Solid Earth

RESEARCH ARTICLE
10.1029/2022JB026016

Hydrogen and Silicon Effects on Hexagonal Close Packed Fe Alloys at High Pressures: Implications for the Composition of Earth's Inner Core

Suyu Fu[1,2], Stella Chariton[3], Vitali B. Prakapenka[3], and Sang-Heon Shim[1]

[1]School of Earth and Space Exploration, Arizona State University, Tempe, AZ, USA, [2]Now at Department of Earth and Planetary Science, The University of Tokyo, Tokyo, Japan, [3]Center for Advanced Radiation Sources, University of Chicago, Chicago, IL, USA

Key Points:

- Equations of state are measured for $Fe_{0.83}Si_{0.17}H_{0.07}$ and $Fe_{0.83}Si_{0.17}H_{0.46}$ alloys in hexagonal close-packed structures
- Inclusion of a H atom in hcp Fe-Si-H alloys results in a volume increase approximately eight times greater than that by a Si atom
- Comparison of laboratory results with seismic data suggests that the Earth's inner core may contain 1.6–3 wt% Si and 0.15–0.6 wt% H

Supporting Information:

Supporting Information may be found in the online version of this article.

Correspondence to:

S. Fu and S.-H. Shim,
fsyxhy@gmail.com;
sshim5@asu.edu

Citation:

Fu, S., Chariton, S., Prakapenka, V. B., & Shim, S.-H. (2023). Hydrogen and silicon effects on hexagonal close packed Fe alloys at high pressures: Implications for the composition of Earth's inner core. *Journal of Geophysical Research: Solid Earth*, *128*, e2022JB026016. https://doi.org/10.1029/2022JB026016

Received 8 NOV 2022
Accepted 10 APR 2023

Author Contributions:

Conceptualization: Suyu Fu, Sang-Heon Shim
Formal analysis: Suyu Fu
Funding acquisition: Sang-Heon Shim
Methodology: Suyu Fu, Stella Chariton, Vitali B. Prakapenka, Sang-Heon Shim
Supervision: Sang-Heon Shim
Validation: Suyu Fu, Sang-Heon Shim
Visualization: Suyu Fu
Writing – original draft: Suyu Fu
Writing – review & editing: Suyu Fu, Stella Chariton, Vitali B. Prakapenka, Sang-Heon Shim

Abstract Hexagonal close-packed (hcp) structured Fe-Ni alloy is believed to be the dominant phase in the Earth's inner core. This phase is expected to contain 4%–5% light elements, such as Si and H. While the effects of individual light element candidates on the equation of state (EoS) of the hcp Fe metal have been studied, their combined effects remain largely unexplored. In this study, we report the equations of state for two hcp-structured Fe-Si-H alloys, namely $Fe_{0.83}Si_{0.17}H_{0.07}$ and $Fe_{0.83}Si_{0.17}H_{0.46}$, using synchrotron X-ray diffraction measurements up to 125 GPa at 300 K. These alloys were synthesized by cold compression of Fe-9wt%Si in either pure H_2 or Ar-H_2 mixture medium in diamond-anvil cells. The volume increase caused by a H atom in hcp Fe-Si-H alloys is approximately eight times greater than that by a Si atom. We used the improved data set to develop a composition-dependent EoS that covers a wide range of compositions. Our calculated density and bulk sound velocity of hcp Fe-Si-H alloys suggest a large trade-off between Si and H contents in fitting the seismic properties of the inner core. Combining our new EoS with geophysical and geochemical constraints, we propose 1.6–3 wt% Si and 0.15–0.6 wt% H in the Earth's inner core.

Plain Language Summary The Earth's inner core is believed to be made up of solid iron and nickel alloys, but there are also some lighter elements alloyed in. We studied how silicon and hydrogen affect the density and sound wave velocity of the iron alloys in the inner core. We combine our new data with existing datasets to create a model that shows that the inner core likely contains around 1.6%–3% silicon and 0.15%–0.6% hydrogen. These amounts can explain the density and sound velocity of the inner core as observed through seismic measurements.

1. Introduction

The Earth's core is believed to primarily consist of Fe-Ni alloy according to cosmoschemical and geochemical constraints (Badro et al., 2015; McDonough & Sun, 1995). However, the seismologically-constrained density of the Earth's core, such as one from the preliminary reference Earth model (PREM) (Dziewonski & Anderson, 1981), is 5%–10% lower than that of Fe and Fe-Ni alloy at the pressure and temperature (*P-T*) conditions expected to the core (Dewaele et al., 2006; Fei et al., 2016; Sakai et al., 2014), which is known as the density deficit (Birch, 1952). Extensive experimental and geochemical studies have proposed different light elements to explain such a density deficit, including silicon (Si), sulfur (S), oxygen (O), carbon (C), and hydrogen (H) (Hirose et al., 2021). Among them, Si and H are important candidates due to their abundances in the Earth system (McDonough & Sun, 1995) and their high solubilities in Fe metal at high *P-T* (Badding et al., 1991; Fischer et al., 2013; Fu et al., 2022, 2023).

Phase diagram of Fe-Si alloys (Fischer et al., 2013; Tateno et al., 2015) indicates that the hexagonal close-packed (hcp) structured phase is stable under the *P-T* conditions expected for the inner core, if the Si content in the region is less than 9 wt%. A recent dynamic compression study showed that the density of Fe-Si alloy containing 3.8 wt% Si can explain the density of the inner core (Huang et al., 2019). However, incorporation of Si alone cannot match the observed low shear wave velocity and high Poisson's ratio of the inner core (Huang et al., 2022). A recent computational study has shown that when H is present a range of the H and Si concentrations can explain the observed density, sound velocities, and Poisson's ratio of the inner core (He et al., 2022; Wang et al., 2021).

There have been a number of experiments on the equations of state of pure Fe metal, FeH_x alloys, and Fe-Si alloys (Dewaele et al., 2006; Edmund et al., 2019; Fei et al., 2016; Fischer et al., 2012, 2014; Miozzi et al., 2020; Pepin et al., 2014). However, studies on the H-bearing hcp Fe-Si alloys are limited (Fu et al., 2022; Tagawa et al., 2016). Pure Fe metal can incorporate a large amount of H and form FeH_x (x could be 1–5) with cold compression in diamond-anvil cells (DACs) up to 130 GPa (Badding et al., 1991; Pepin et al., 2017). Tagawa et al. (2016) conducted laser heating on Fe-6.5wt%Si (6.5 wt% Si, $Fe_{0.88}Si_{0.12}$) in a H medium to temperatures lower than 1000 K in DACs and reported the pressure–volume (P-V) data of the hcp H-bearing Fe-6.5wt%Si alloys. Formation of H-bearing Fe-9wt%Si (9 wt% Si, $Fe_{0.83}Si_{0.17}$) was documented at pressures above ~11 GPa after cold-compression of the sample in a H medium in DACs (Fu et al., 2022). However, the data set does not cover sufficiently large ranges of H and Si contents to allow for the evaluation of their combined effects on the density and elasticity of hcp Fe-Si-H alloys to better constrain the composition of the inner core.

We synthesized $Fe_{0.83}Si_{0.17}H_x$ ($x = 0.07$ and 0.46) by compressing Fe-9wt%Si in a medium of pure H_2 or Ar-H_2 mixture in DACs at room temperature. We measured the volume of the H-bearing Fe-9wt%Si alloys up to 125 GPa at room temperature using synchrotron X-ray diffraction (XRD). Our data are fit together with the existing experimental datasets to evaluate the combined effects of Si and H on the equation of state (EoS) of hcp Fe-Si-H alloys (Dewaele et al., 2006; Fu et al., 2022; Pepin et al., 2014; Tagawa et al., 2016). Our new EoS, which takes into account the combined effects of Si and H, was used to calculate the density and bulk sound velocity of the alloys at the P-T conditions expected for the inner core. By comparing the calculated properties to the seismic observations, we provide improved constraints on possible concentrations of Si and H in the Earth's inner core.

2. Methods

The starting Fe-Si alloy sample was purchased from GoodFellow Corporation. Electron probe micro-analyses (EPMA) show that the sample is homogeneous and has a composition of Fe-9wt%Si or $Fe_{0.83}Si_{0.17}$ (8.84 ± 0.30 wt% Si) (Fu et al., 2022). The average grain size was 3–5 μm (Fu et al., 2022; Huang et al., 2019). Re gaskets with initial thicknesses of 250 μm were pre-indented into ~20 μm using symmetric DACs with culet sizes between 200 μm flat and 120 μm beveled. We drilled holes with diameters of 60% of the culet sizes in the pre-indented areas for the sample chambers. The Fe-9wt%Si alloy was compressed into a 7-μm thin foil and loaded into the prepared sample chambers for high-pressure experiments. Small pieces of Au and ruby were placed close to the sample foil as pressure calibrants (Figure S1 in Supporting Information S1) (Shen et al., 2020; Ye et al., 2018). Pressure and its uncertainty were calculated based on the measured unit-cell volumes of Au before and after each measurement.

Either pure H_2 gas or Ar-H_2 mixture was loaded into the sample chambers as a pressure transmitting medium as well as a hydrogen source by using a gas loading system at Arizona State University. The use of the Ar-H_2 mixture reduces the H supply to the sample so that the Fe-9wt%Si alloy can incorporate different amount of H into its structure. In addition, pure H can damage anvils easily because of H diffusion into the diamond anvils under high pressure, while Ar in the Ar-H_2 mixture reduces H diffusion and therefore the likelihood of diamond breakage in high-pressure experiments. Three DACs were prepared: DAC #1 was loaded with pure H_2, while DACs #2 and #3 were loaded with an Ar-H_2 mixture containing 60%–70% H_2 (refer Fu et al., 2023 for detail). We note that pure H_2 is compressible and can provide a low deviatoric stress environment at high pressures. For experiments with an Ar-H_2 pressure medium, Ar could be an important factor for deviatoric stress. We calculated the uniaxial stress component (t) of Au by following the procedure in earlier studies (Singh et al., 1998; Takemura & Dewaele, 2008). The t can be related as $t = \sigma_3 - \sigma_1$, where σ_3 and σ_1 are stress components in axial and radial directions, respectively. The estimated t is less than 1.2 GPa at the highest pressure of our experiments. The t value is slightly higher but comparable to the value reported for a He medium (up to ~0.89 GPa at 123 GPa) in Takemura and Dewaele (2008) (Figure S2 in Supporting Information S1). Therefore, a reasonable estimation for pressure uncertainty is 3%.

High-pressure XRD experiments were performed on the H-bearing Fe-9wt%Si at the 13-IDD beamline of the GeoSoilEnviroCARS (GSECARS) sector of the Advanced Photon Source (APS), Argonne National Laboratory (ANL). We used an incident monochromatic X-ray beam with a wavelength of 0.3344 Å and a spot size of 3×4 μm^2. The DACs were first compressed to ~30 GPa to promote H into the crystal structure of Fe-9wt%Si alloys at high pressures. We did not laser anneal the sample to prevent over-hydrogenation of the samples. The Fe-Si-H alloys in this study were all formed at 300 K by cold compression. XRD data were collected at the same

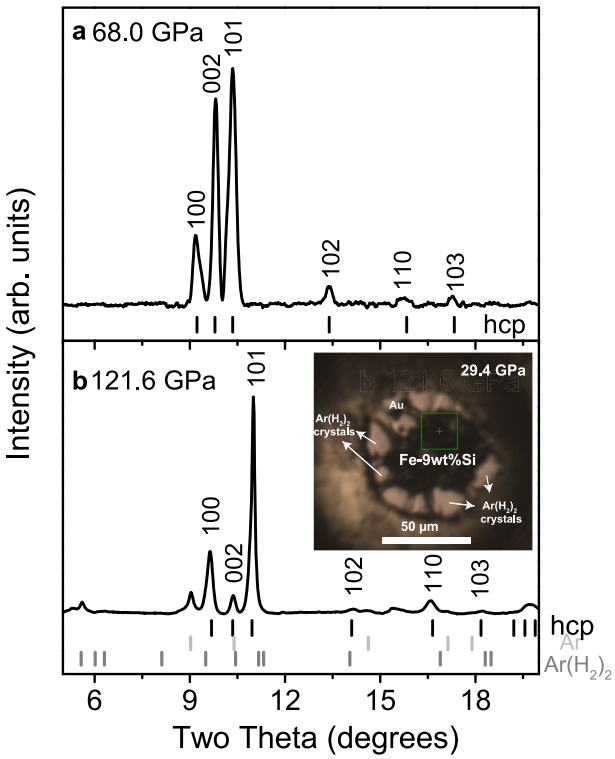

Figure 1. X-ray diffraction patterns of Fe-9wt%Si alloy in a H-bearing medium at high pressures and 300 K. (a) 68.0 GPa in a pure H_2 medium; (b) 121.6 GPa in an Ar-H_2 mixture medium. The diffraction lines are labeled with their Miller indices. The vertical ticks show the peak positions of hcp (black), Ar (light gray) and $Ar(H_2)_2$ (gray). Ar and H_2 react and form $Ar(H_2)_2$ crystals (Ji et al., 2017) at pressures above 4.2 GPa and room temperature. The inset in (b) shows a microscope image of the sample in an Ar-H_2 medium at 29.4 GPa. The boundary of $Ar(H_2)_2$ crystals can be seen in the transparent area around the sample. The wavelength of the incident X-ray beam is 0.3344 Å.

spot up to 125 GPa at room temperature (Table S1 in Supporting Information S1). DIOPTAS software (Prescher & Prakapenka, 2015) was used to integrate XRD patterns, and PeakPo software (S. Shim, 2017) was employed to identify the diffraction peaks. In PeakPo, the diffraction peaks were individually fit to pseudo-Voigt profile function. The fitted peak positions were then used for the unit-cell parameter fitting together with their Miller indices in PeakPo following the method in Holland and Redfern (1997). The volume in a unit of $Å^3$/(# of Fe + Si Atoms) is used in this study for direct comparison among different compositions (volume per total Fe and Si atoms in a unit cell, # means number).

3. Results and Discussion

3.1. X-Ray Diffraction Observations

X-ray diffraction patterns show that the cold-compressed Fe-9wt%Si in H-bearing media has a hcp structure between 31 and 125 GPa (Figure 1). When pure H is used as a medium, we only observed peaks from the hcp phase (Figure 1a). In DACs #2 and #3 where an Ar-H_2 medium was used, diffraction peaks of Ar or $Ar(H_2)_2$ were also observed (Figure 1b). Earlier experiments showed that a hexagonal-structured $Ar(H_2)_2$ phase can crystallize from an Ar-H_2 mixture above 4.2 GPa at room temperature (Ji et al., 2017; Loubeyre et al., 1994). The unit-cell volumes of the observed Ar and $Ar(H_2)_2$ phases are consistent with previous reports (Finger et al., 1981; Ji et al., 2017) within the experimental uncertainties (Figure S3 in Supporting Information S1).

The cold-compressed Fe-9wt%Si alloys in DACs #1 and #3 display 10%–14% and 1.5%–2.5% higher unit-cell volumes than H-free Fe-9wt%Si (Tateno et al., 2015), respectively (Figure 2 and Table S1 in Supporting Information S1). In contrast, the sample in DAC #2 does not show a volume expansion. XRD patterns are dominated by sharp and intense diffraction peaks from the hcp alloy without major peak overlaps. The uncertainties estimated for the volume including those from peak fitting and unit-cell fitting are less than 0.6%. Studies have shown that H can enter the crystal structures of metallic Fe or Fe-Si alloy at high pressures and room temperature, causing a volume expansion (Badding et al., 1991; Fu et al., 2022; Pepin et al., 2014). Thus, we attribute the observed volume expansions in Fe-9wt%Si to H incorporation. The expanded unit-cell volume observed for the sample in DAC #1 can be understood from a larger amount of H in the alloy formed from a greater amount of H available in the setup. Even though both DACs #2 and #3 were loaded with the same procedure for an Ar-H_2 mixture, the Fe-9wt%Si alloys have different volumes. Under microscope, we found the formation of large $Ar(H_2)_2$ single crystals in DACs during cold compression (Figure 1b inset). The local concentration of hydrogen near the sample was likely different depending on the location of the $Ar(H_2)_2$ crystals in the sample chamber. This is because the $Ar(H_2)_2$ crystals would have acted as a barrier to the hydrogen diffusion, preventing it from reaching all parts of the sample evenly. As a result, the amount of hydrogen available for the hydrogenation of Fe-9wt%Si would have been different between DACs #2 and #3.

3.2. Equation of State Fitting for Individual Compositions

The pressure-volume data of the H-bearing Fe-9wt%Si alloys from our experiments are individually fit to the third-order Birch-Murnaghan equation (Birch, 1947):

$$P = \frac{3}{2}K_0\left[(V_0/V)^{\frac{7}{3}} - (V_0/V)^{\frac{5}{3}}\right]\left\{1 + \frac{3}{4}\left(K_0' - 4\right)\left[(V_0/V)^{\frac{2}{3}} - 1\right]\right\} \quad (1)$$

where V and V_0 are volumes at high pressure and ambient conditions, respectively, and K_0 and K_0' are the isothermal bulk modulus and its pressure derivative at ambient conditions, respectively. Because the H-bearing Fe alloys

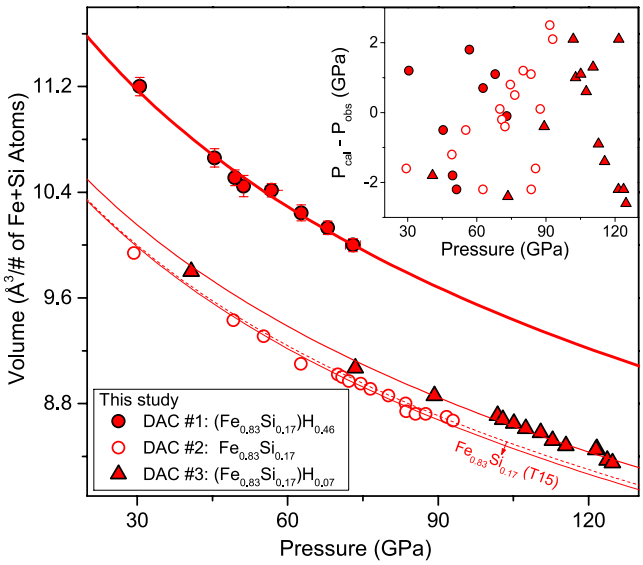

Figure 2. Volume of hcp Fe-Si-H alloy at high pressures. Solid circles: diamond-anvil cell (DAC) #1 with a pure H_2 medium; open circles and solid triangles: DACs #2 and #3, respectively, with a medium of Ar-H_2 mixture. The solid lines are the Birch-Murnaghan equation of state (EoS) fits to the experimental data of each phase individually. The dashed red line is the EoS data of H-free hcp Fe-9wt%Si ($Fe_{0.83}Si_{0.17}$, T15) from previous experiments (Tateno et al., 2015), which agree well with our data from DAC #2. The inset shows the fit residues in pressure. The small fit residues indicate that the H contents in the alloys may not change with pressure after initial hydrogenation.

can lose H during decompression to ambient pressure, particularly pressures lower than 5 GPa (Badding et al., 1991), we fit the data points above 30 GPa only. Considering the trade-off between parameters (V_0, K_0, and K_0') in the EoS fitting, K_0' is fixed to 4.88, same as that of H-free Fe-9wt%Si (Tateno et al., 2015). The best fit results are: V_0 = 12.75(16) Å^3/(# of Fe + Si Atoms) and K_0 = 168(6) GPa, V_0 = 11.32(18) Å^3/(# of Fe + Si Atoms) and K_0 = 176(9) GPa, and V_0 = 11.47(12) Å^3/(# of Fe + Si Atoms) and K_0 = 184(6) GPa for DACs #1, #2, and #3, respectively (Table 1). The EoS parameters obtained for the hcp alloy from DAC #2 are consistent with those of H-free Fe-9wt%Si (Tateno et al., 2015), supporting a negligible amount of H in the sample. The small fit residues found for the data from all three different experiments suggest that the pressure-volume data of the Fe-Si-H alloys can be well described by the Birch-Murnaghan equation (Figure 2). The results also indicate that the H content of the alloys may not change with pressure. The *c/a* ratio of the H-bearing Fe-9wt%Si alloys measured in this study is more similar to that of H-free Fe-9wt%Si (Tateno et al., 2015) than that of Fe metal, although it is difficult to be conclusive because of the data scatter. Therefore, we interpret that H does not change the axial ratio of the hcp Fe-Si alloys within uncertainties (Figure S4 and Table S1 in Supporting Information S1).

3.3. Estimation of Hydrogen Contents in hcp Fe-Si-H Alloys

The contents of hydrogen stored in a metal alloy (x) can be estimated from the volume expansion by hydrogenation (Fukai, 1992): $x = (V_{MH_x} - V_M)/\Delta V_H$, where ΔV_H, V_{MH_x}, and V_M are the volume increase per H atom, the volume of metal hydride (MH_x), and the volume of H-free metal (M), respectively. The volume differences between H-bearing Fe-9wt%Si (this study) and H-free Fe-9wt%Si (Tateno et al., 2015) are almost constant at 0.15 and 1.02 Å^3/(# of Fe + Si Atoms) for the samples in DACs #3 and #1, respectively (Figure 3b). Therefore, we assumed that x does not change once an alloy forms. Because experimental constraints on the value of ΔV_H are still lacking for Fe-Si-H alloys, we assumed

Table 1
Static Equation of State Parameters of hcp Fe-Si-H Alloys

Composition	V_0 (Å^3)	K_0 (GPa)	K_0'
$Fe_{0.83}Si_{0.17}H_{0.46}$ (DAC #1, this study)	12.75(16)	168(6)	4.88(fixed)
$Fe_{0.83}Si_{0.17}$ (DAC #2, this study)	11.32(18)	176(9)	4.88(fixed)
$Fe_{0.83}Si_{0.17}H_{0.07}$ (DAC #3, this study)	11.46(12)	184(6)	4.88(fixed)
$Fe_{0.83}Si_{0.17}H_{0.23}$ (Fu et al., 2022)	12.1(fixed)	150(6)	5.1(4)
$Fe_{0.83}Si_{0.17}$ (Tateno et al., 2015)$^{\#}$	11.35(10)	179.6(42)	4.88(11)
$Fe_{0.88}Si_{0.12}$ (Tateno et al., 2015)$^{*,\#}$	11.31	170.9(15)	5.04(5)
$Fe_{0.88}Si_{0.12}H_{0.56}$ (Tagawa et al., 2016)$^{\#}$	12.44(6)	236(13)	4.34(21)
$Fe_{0.88}Si_{0.12}H_{0.74}$ (Tagawa et al., 2016)$^{\#}$	12.9(5)	241(6)	4.1(4)
$Fe_{0.90}Si_{0.10}$ (Edmund et al., 2019)	11.26(5)	172.4(60)	4.64(14)
Fe (Dewaele et al., 2006)	11.234(12)	165.5(52)	4.99(16)
Fe (Fei et al., 2016)	10.09	191(5)	4.5(1)
Fe (Miozzi et al., 2020)	11.4(1)	129(6)	6.2(2)
dhcp FeH (Pepin et al., 2014)	13.91(4)	135.5(30)	4.36(9)

Note. Some previous experimental data were refit using third order Birch-Murnaghan EoS for consistency (labeled with $^{\#}$). For *, parameters are obtained by using linear interpolation between pure hcp Fe metal (Dewaele et al., 2006) and Fe–9wt%Si (Tateno et al., 2015). V_0 is the atomic volume in Å^3/# of Fe + Si Atoms.

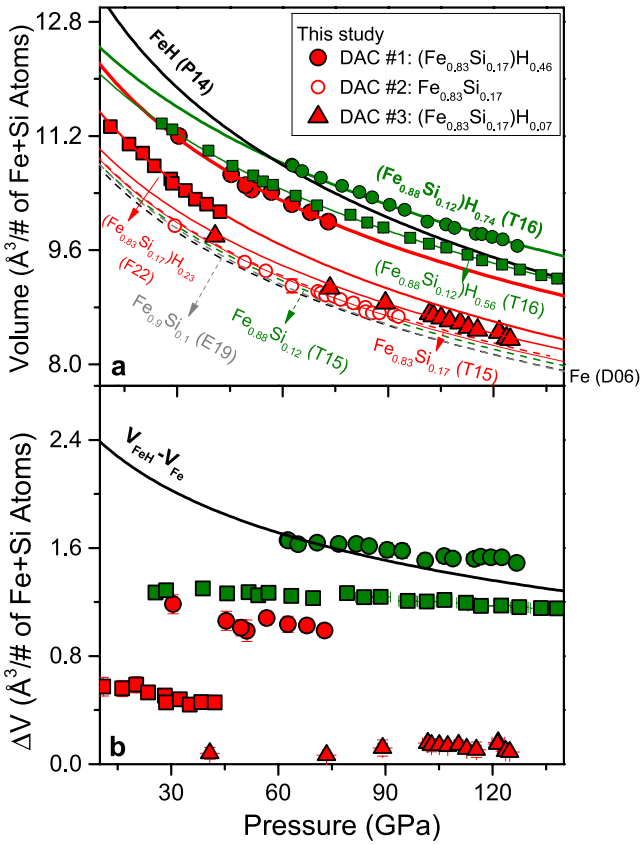

Figure 3. (a) Pressure-volume relationships of hcp Fe-Si-H alloys at high pressures. The red symbols are the H-bearing hcp Fe-9wt%Si in three diamond-anvil cell (DAC) runs from our study. Solid circles: DAC #1 with a pure H_2 medium; open circle and solid triangles: DACs #2 and #3, respectively, with a medium of Ar-H_2 mixture. The solid lines are the Birch-Murnaghan equation of state (EoS) fit to the experimental data. The solid thin red line is the best fits for the data points from DAC #2 which agrees well with the EoS of H-free hcp Fe-9wt%Si (dashed red line, T15) (Tateno et al., 2015). The EoS's of hcp Fe-Si-H alloys with different Si and H contents are included for comparison: Fe (dashed black, D06) (Dewaele et al., 2006), dhcp FeH (solid black, P14) (Pepin et al., 2014), $Fe_{0.9}Si_{0.1}$ (dashed gray, E19) (Edmund et al., 2019), $Fe_{0.88}Si_{0.12}$ (dashed olive, T15) (Tateno et al., 2015), $Fe_{0.83}Si_{0.17}$ (dashed red, T15) (Tateno et al., 2015), $Fe_{0.88}Si_{0.12}H_{0.56}$ and $Fe_{0.88}Si_{0.12}H_{0.74}$ (olive squares and circles, T16) (Tagawa et al., 2016), $Fe_{0.83}Si_{0.17}H_{0.23}$ (red squares, F22) (Fu et al., 2022). We used black, olive, and red for the alloys with three different Si contents (0%, 6.5 wt%, and 9 wt% Si, respectively). Curves changing from dashed to thin solid, then to thick solid indicate increasing hydrogen contents (x ranges from 0 to 1) in the alloys. (b) Volume expansion of the H-bearing hcp Fe-Si alloys with respect to H-free alloy phases for the estimation of H content. ΔV is calculated from $V((Fe_{1-y}Si_y)H_x) - V(Fe_{1-y}Si_y)$.

$\Delta V_H = 2.2$ Å^3/Atoms from Antonov et al. (2019), which is estimated for the close-packed structures of Fe-H alloys. Such an assumption is reasonable because in the hcp Fe-Si-H alloy the Si substitutes for Fe while H exists in the interstitial sites (Martorell et al., 2016; Pepin et al., 2014). In addition, the Si effect on the volume of hcp Fe-Si alloys is relatively small (Figure 3a) (Dewaele et al., 2006; Tateno et al., 2015). Therefore, the effect of H on hcp Fe and Fe-Si alloys can be similar. Calculations show the H-bearing alloys from DACs #1 and #3 have compositions of $(Fe_{0.83}Si_{0.17})H_{0.46}$ and $(Fe_{0.83}Si_{0.17})H_{0.07}$, respectively. The measured volumes of the sample have small uncertainties (<0.6% errors). The major uncertainty source for the estimated hydrogen contents is the value of ΔV_H. A variation of 0.2 Å^3/Atoms in ΔV_H (Antonov et al., 2019; Fukai, 1992) yields a 10% change in the H contents. There are a few estimations for ΔV_H and often slightly different values have been used. For consistency, the H contents of the hcp Fe-Si-H reported in Tagawa et al. (2016) and Fu et al. (2022) are corrected for the ΔV_H from Antonov et al. (2019) (Figure 3b). Pure Fe metal under H-saturated conditions forms stoichiometric dhcp FeH (therefore $x = 1$) at pressures above 3.5 GPa and room temperature (Badding et al., 1991; Pepin et al., 2014). In contrast, we found that the H solubility in Fe-9wt%Si and Fe-6.5wt%Si (Tagawa et al., 2016) is much smaller even in a pure H medium. Overall, these observations indicate that Si in Fe metal decreases the solubility of H into the crystal structure of Fe metal alloys.

3.4. Effects of H and Si on the Equations of State of hcp Fe-Si-H Alloys

By combining our data with the earlier experimental data on H-bearing and H-free Fe-Si alloys with different compositions (Dewaele et al., 2006; Edmund et al., 2019; Fu et al., 2022; Pepin et al., 2014; Tagawa et al., 2016; Tateno et al., 2015), we obtained the effects of Si and H on the EoS of the hcp Fe-H-Si alloys. There are multiples of studies on Fe-9wt%Si (Fischer et al., 2014; Tateno et al., 2015) and pure Fe metal (Dewaele et al., 2006; Fei et al., 2016; Miozzi et al., 2020). We chose the data by Tateno et al. (2015) for Fe-9wt%Si up to 300 GPa at 300 K. The data are consistent with Fischer et al. (2014) which focused more on high-temperature P-V data. For the Fe metal, recent experiments are consistent with each other within 2% (Dewaele et al., 2006; Fei et al., 2016; Miozzi et al., 2020). Dewaele et al. (2006) reported a dense P-V data set up to 200 GPa at 300 K measured in a He pressure medium which is known to provide quasi-hydrostatic stress conditions. Gold is used as the pressure scale in this study and most of the existing datasets for hcp H-bearing $Fe_{0.83}Si_{0.17}$ and dhcp FeH (Fu et al., 2022; Pepin et al., 2014). MgO, B2-NaCl, and B2-KCl were used as pressure scales in Tateno et al. (2015), Tagawa et al. (2016), and Edmund et al. (2019). In our study, their reported pressures were corrected for the internally consistent pressure scales (Dorfman et al., 2012; Fei et al., 2007; Ye et al., 2018). Therefore, the pressures determined from different pressure calibrants should be consistent within ±3 GPa at megabar pressure (Dorfman et al., 2012; Fei et al., 2007; Ye et al., 2018).

For the H-free system, hcp Fe shows a slight volume increase, less than 2%, with an increase in Si content from 0% to 17% (Figure 3a). In contrast, when H was incorporated, volume increases much more significantly, up to 20% from pure Fe metal to dhcp FeH. We assumed a linear effect of Si and H on the V_0 of hcp Fe-Si-H alloys:

$$V_0(\mathrm{Si,H}) = 11.26(6) + 0.31(9)y + 2.56(8)x \quad (2)$$

where $(Fe_{1-y}Si_y)H_x$ formulation is used. The reason is that Si atoms replace Fe atoms directly while H atoms enter the interstitial sites of the hcp crystal structure (Martorell et al., 2016; Pepin et al., 2014). The equation

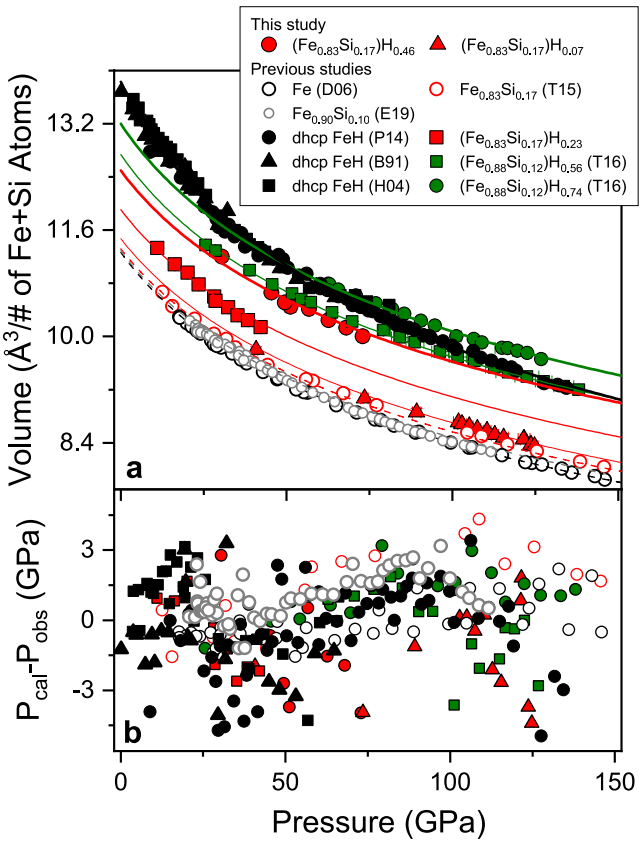

Figure 4. Fit results for the combined effects of Si and H on the high-pressure volumes of hcp Fe-Si-H alloys. (a) Pressure-volume relationship of hcp Fe-Si-H alloys. The symbols are for the experimental data points, while the curves are for the best fit using Equations 5 and 6. The solid red triangles and circles are for $Fe_{0.83}Si_{0.17}H_{0.07}$ and $Fe_{0.83}Si_{0.17}H_{0.46}$, respectively, in this study. The others are from the previous experiments: Fe (open black circle, D06) (Dewaele et al., 2006), dhcp FeH (solid black circles, P14; black triangle, B91; black squares, H04) (Badding et al., 1991; Hirao et al., 2004; Pepin et al., 2014), $Fe_{0.9}Si_{0.1}$ (open gray circles, E19) (Edmund et al., 2019), $Fe_{0.88}Si_{0.12}H_{0.56}$ and $Fe_{0.88}Si_{0.12}H_{0.74}$ (olive squares and circles, respectively, T16) (Tagawa et al., 2016), $Fe_{0.83}Si_{0.17}$ (open red circles, T15) (Tateno et al., 2015), and $Fe_{0.83}Si_{0.17}H_{0.23}$ (red squares, F22) (Fu et al., 2022). (b) Fit residues in pressure for the best fit. P_{cal} and P_{obs} are calculated and measured pressures, respectively.

above predicts 11.26(6) Å^3/Atoms for pure Fe metal in hcp which agrees with the existing projection of the value to 1 bar (11.214(49) Å^3/Atoms) within the experimental uncertainties (Dewaele et al., 2006).

The combined Si and H effects on K_0 and K_0' of the hcp alloys are more complicated. Without Si, both K_0 and K_0' of hcp Fe decrease with an increase in H content. However, for Fe-6.5wt%Si, K_0 increases with the H incorporation (Figure S5 in Supporting Information S1 and Table 1). In comparison, K_0 decreases with an increasing H content in the Fe-9wt%Si alloy (Figure S5 in Supporting Information S1). Therefore, a linear relationship is not sufficient to evaluate the Si and H effects on the K_0 and K_0' of hcp Fe-Si-H alloys. Also, because of well-known trade-offs between K_0 and K_0' in fitting individual compositions, it is difficult to use a linear relationship (Jackson & Rigden, 1996). Here, we used the following equations to fit all the experimental data together:

$$K_0(Si,H) = K_0 + \frac{\partial K_0}{\partial y}y + \frac{\partial K_0}{\partial x}x + \frac{\partial^2 K_0}{\partial x \partial y}xy \quad (3)$$

$$K_0'(Si,H) = K_0' + \frac{\partial K_0'}{\partial y}y + \frac{\partial K_0'}{\partial x}x + \frac{\partial^2 K_0'}{\partial x \partial y}xy \quad (4)$$

where $\frac{\partial K_0}{\partial y}$, $\frac{\partial K_0}{\partial x}$, $\frac{\partial K_0'}{\partial y}$, and $\frac{\partial K_0'}{\partial x}$ are the first-order Si and H effects on K_0 and K_0', respectively, and $\frac{\partial^2 K_0}{\partial x \partial y}$ and $\frac{\partial^2 K_0'}{\partial x \partial y}$ are the second-order coefficients due to the possible interactions between Si and H. The best fit yields:

$$K_0(Si,H) = (162 \pm 3) + (96 \pm 12)y - (25 \pm 3)x + (250 \pm 30)xy \quad (5)$$

$$K_0'(Si,H) = (5.02 \pm 0.08) - (0.24 \pm 0.18)y - (0.57 \pm 0.12)x + (10 \pm 3)xy \quad (6)$$

The fit residuals in pressure are less than ±3 GPa (Figure 4b). To ensure consistency, we calculated K_0 and K_0' predicted from our fitting results for Fe-Si-H alloys with different compositions and compare them with the values obtained from the individual fits in the previous section. They agree well considering the trade-offs between the parameters (Table 1). That is, our models can reproduce the experimental data points of Fe-Si-H alloys with different Si and H contents (Dewaele et al., 2006; Edmund et al., 2019; Fu et al., 2022; Pepin et al., 2014; Tagawa et al., 2016; Tateno et al., 2015) (Figure 4a). Much larger pressure residuals (~13 GPa) were found if we ignore $\frac{\partial^2 K_0}{\partial x \partial y}$ and $\frac{\partial^2 K_0'}{\partial x \partial y}$ (Figure S6 in Supporting Information S1). Therefore, the second-order coefficients from Si-H interactions are necessary to properly model the combined Si and H effects.

4. Implications for the Composition of the Earth's Inner Core

The Earth's solid inner core is mainly made of hcp Fe-Ni alloy with 4–5 wt% light elements (Hirose et al., 2021; Tateno et al., 2015; Wang et al., 2021). By taking advantage of the equations of state we constructed for the combined Si and H effects on hcp Fe-Si-H alloys, we can make improved calculation on the density (ρ) and bulk sound velocity (V_Φ) for the hcp alloys with varying Si and H contents. The calculated properties can be then compared with those from the seismic measurements (PREM in this case) (Dziewonski & Anderson, 1981), which allows for the estimation of the Si and H contents in the inner core.

We assume that Si and H are the two major light elements in the inner core. Mie-Gruneisen thermal EoS is employed to calculate ρ and V_Φ of hcp FeSi-H alloys at the P-T conditions expected for the inner core (see Supporting Information S1 for details) (Cottaar et al., 2014; Jackson & Rigden, 1996; Stixrude & Lithgow-Bertelloni, 2005). In this model, thermal behavior can be described by Debye temperature (θ_0), Grüneisen parameter at ambient conditions

Table 2
Parameters for the Thermal Equation of State of hcp Fe-Si-H Alloys With Different Compositions

	θ_0 (K)	γ_0	q_0
Fe-Si-H alloys (used in this study)	417*	1.59*	1*
$Fe_{0.90}Si_{0.10}$ (Edmund et al., 2019)	422*	1.72(13)	0.65(23)
$Fe_{0.83}Si_{0.17}$ (Fischer et al., 2014)	417*	1.14(0.14)	1*
$Fe_{0.73}Si_{0.27}$ (Fischer et al., 2012)	417*	1.8(1)	1*
Fe (Fei et al., 2016)	422*	1.74	0.78
Fe (Miozzi et al., 2020)	420*	1.11(1)	0.3(3)
Fe (Morrison et al., 2019)	417*	2.04(1)	1*
$Fe_{0.91}Ni_{0.09}$ (Morrison et al., 2019)	417*	2.07(2)	1*
$Fe_{0.8}Ni_{0.1}Si_{0.1}$ (Morrison et al., 2019)	417*	2.03(5)	1*

Note. The values marked with * are fixed during fitting.

(γ_0), and a volume-independent constant (q_0). Because high-temperature volume measurements do not exist for hcp Fe-Si-H at high pressures, we consider thermal parameters of hcp Fe and Fe-Si alloys (Edmund et al., 2019; Fei et al., 2016; Fischer et al., 2012, 2014; Miozzi et al., 2020; Morrison et al., 2019). Existing experimental data for Fe-Si alloys show that Si content does not change θ_0, γ_0, and q_0 significantly (Table 2). Therefore, we assume that these three thermal parameters for the hcp Fe-Si-H alloys are the same as those of Fe-Si alloys. To examine how the uncertainties of the thermal parameters can affect the results, we examined cases for 30% variations in θ_0, γ_0, and q_0. The variations result in uncertainties less than 0.8% for ρ and V_Φ (Figure S7 in Supporting Information S1). The uncertainty could be larger if uncertainties of three parameters are considered simultaneously. However, with error propagation, uncertainties are likely less than 1.5%. The small impact from the uncertainties of thermal parameters is reasonable because pressure makes much more severe impacts on the properties at the conditions of the inner core and the trade-off among these parameters is large (Shim & Duffy, 2000).

Density and bulk sound velocity profiles of hcp Fe-Si-H alloys are calculated for four different Si contents from our fitting results along the adiabatic temperature profiles of the inner core: FeH_x, $(Fe_{0.97}Si_{0.03})H_x$, $(Fe_{0.94}Si_{0.06})H_x$, and $(Fe_{0.91}Si_{0.09})H_x$. We set the anchor temperature at the boundary between the inner core and the outer core (T_{ICB}) to 5500 K and a Grüneisen parameter to 1.5 (Vocadlo et al., 2003). The comparison found that the density-velocity profiles of hcp Fe-Si-H alloys generally exhibit greater slopes than PREM (Figure 5). Therefore, we consider a range of the H contents for a hcp alloy with a fixed Si content. However, we do not rule out the possibility that both Si and H contents change with depths.

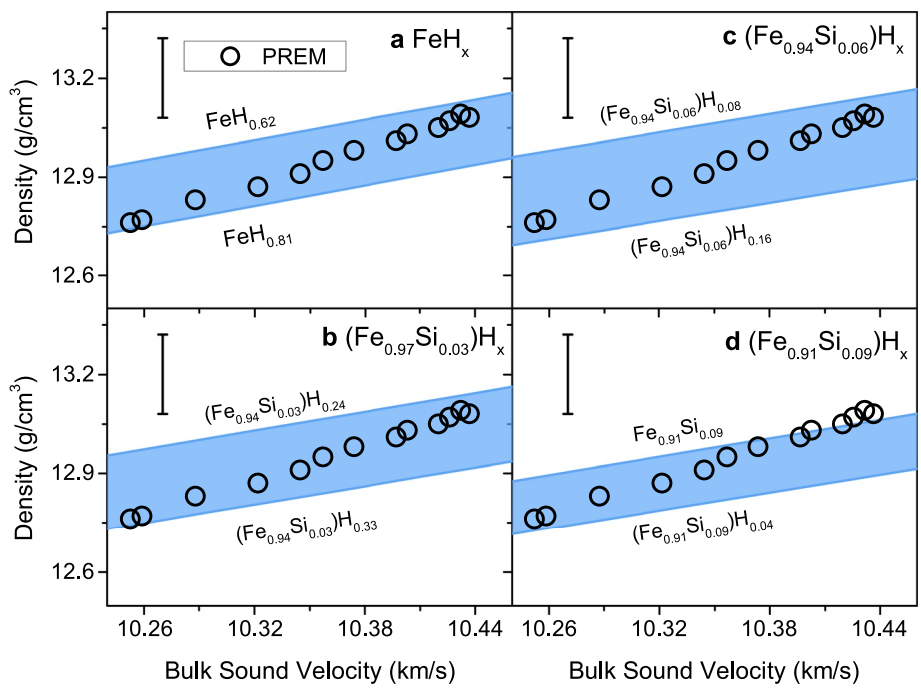

Figure 5. The density and the bulk sound velocity of hcp Fe-Si-H alloys compared with the seismic profiles of the Earth's inner core (preliminary reference Earth model (PREM)). (a) FeH_x; (b) $(Fe_{0.97}Si_{0.03})H_x$; (c) $(Fe_{0.94}Si_{0.06})H_x$; (d) $(Fe_{0.91}Si_{0.09})H_x$. The properties were calculated for the pressure and temperature conditions that are relevant to the Earth's inner core, along an adiabatic temperature profile (T_{ICB} = 5500 K). The circles are from the PREM model (Dziewonski & Anderson, 1981). The vertical ticks are the estimated uncertainties.

Our results show a large trade-off between the Si and H contents. For instance, if there is no Si in the inner core, as much as 1.10–1.43 wt% H is required to match the density and the bulk sound velocity in the region. With Si content increasing to 1.5 and 3.1 wt%, the possible H contents in the inner core decrease to 0.43–0.60 and 0.15–0.3 wt%, respectively. The density and the bulk sound velocity of $Fe_{0.91}Si_{0.09}$ (about 4.7 wt% Si) are comparable to those of Earth's inner core. The fit to PREM becomes worse with further increasing the Si content, indicating that the Si content of the inner core should be less than 4.7 wt%. That is, the maximum Si and H contents in inner core are approximately 4.7 and 1.43 wt%, respectively.

There are some uncertainties in the temperature profile of the inner core. Therefore, we calculated the effect of temperature on ρ and V_Φ of hcp Fe-Si-H alloys, and tested how the estimated H and Si contents in the Earth's inner core can change with temperature profile. Calculations were conducted for three adiabatic geotherms with T_{ICB} = 4700 K, 5500 K, and 6300 K. With an 800-K increase in temperature profile, ρ and V_Φ decrease by approximately 0.4% (see Figure S8 in Supporting Information S1). Our analysis on the combined Si and H effects suggests that 1 mol% increase in the H content of the hcp Fe-Si-H alloy decreases the ρ and V_Φ by 0.1%–0.2% (see Section 3.4). That is, if the temperature of the inner core increases (decreases) by 800 K, the estimated H contents for a fixed Si content in the region would decrease (increase) by 2–4 mol% (0.04–0.08 wt%).

Because the solid inner core crystallizes and grows in the liquid metal during the cooling of Earth (Jacobs, 1953), the light element concentrations can be constrained by their partitioning between solid and liquid (Jephcoat & Olson, 1987). Recent models considering both geochemical and geophysical constraints (Badro et al., 2015) suggest that the outer core contains 2–3.6 wt% Si. In addition, theoretical calculations show that the solid-liquid partitioning coefficient of Si in Fe metal is approximately 1.2 (Alfe et al., 2002). Therefore, the Si content in the inner core can be 1.6–3 wt%. For this amount, our model finds 0.15–0.6 wt% H in the inner core (Figure 5). It should be noted that 0.3–0.6 wt% H has been suggested to be incorporated into the Earth's core during differentiation of an early magma ocean (Tagawa et al., 2021). Then H incorporation into solid inner core can be controlled by the H partitioning between solid and liquid Fe alloys. Some recent studies proposed Fe-FeH phase diagram below 100 GPa (Tagawa et al., 2022). According to the phase diagram, up to 0.42 wt% H can be partitioned into the solid inner core. These H contents estimated from other constraints overlap with what our model found for the Earth's inner core. It is important to note that our estimations here do not include other light elements candidates, such as O, C, and S. Compared with S and Si, O is highly incompatible with the solid Fe metal (Alfe et al., 2002; Badro et al., 2007). Therefore, only a trace amount of O may exist in the inner core. To further improve the constraints on the Si and H contents in the core, future studies should explore combined Si and H effects on the thermal parameters. It is also important to measure the combined effects of Si and H on the shear properties of hcp Fe-rich alloys.

5. Conclusions

Cold compression of Fe-9wt% alloys in a pure H or Ar-H_2 mixture medium results in formation of $Fe_{0.83}Si_{0.17}H_{0.07}$ and $Fe_{0.83}Si_{0.17}H_{0.46}$ alloys at high pressures. The equations of state for these alloys were measured up to 125 GPa at 300 K. Fitting of our new data combined with the previous results (Dewaele et al., 2006; Edmund et al., 2019; Fu et al., 2022; Pepin et al., 2014; Tagawa et al., 2016; Tateno et al., 2015) on Fe-H, Fe-Si, and Fe-Si-H was conducted for investigating the combined impact of Si and H on the EoS of hcp Fe-Si-H alloy. The density and the bulk sound velocity calculated from the EoS of hcp Fe-Si-H alloy were then compared with the seismic properties of the inner core. Combined with geophysical and geochemical constraints (Badro et al., 2015), we propose 1.6–3 wt% Si and 0.15–0.6 wt% H in the Earth's inner core.

Conflict of Interest

The authors declare no conflicts of interest relevant to this study.

Data Availability Statement

All the experimental new data was archived in Zenodo: https://doi.org/10.5281/zenodo.7668928. All the data are provided in tables in the Supporting Information S1 temporarily for review purposes.

Acknowledgments
We thank an anonymous reviewer and Dr. Y. Fei for questions and comments which improved this paper. This work is supported by NSF-Astronomical Science (AST200567 and AST2108129) and NSF-Earth Science (EAR1921298). The authors acknowledge the support of GeoSoilEnviroCARS (University of Chicago, Sector 13) for synchrotron experiments. GeoSoilEnviroCARS was supported by the National Science Foundation—Earth Sciences (EAR-1634415). This research used resources of the Advanced Photon Source, a U.S. Department of Energy (DOE) Office of Science User Facility operated for the DOE Office of Science by Argonne National Laboratory under Contract No. DE-AC02-06CH11357.

References

Alfe, D., Gillan, M., & Price, G. D. (2002). Composition and temperature of the Earth's core constrained by combining ab initio calculations and seismic data. *Earth and Planetary Science Letters*, *195*(1–2), 91–98. https://doi.org/10.1016/s0012-821x(01)00568-4

Antonov, V. E., Gurev, V. M., Kulakov, V. I., Kuzovnikov, M. A., Sholin, I. A., & Zuykova, V. Y. (2019). Solubility of deuterium and hydrogen in fcc iron at high pressures and temperatures. *Physical Review Materials*, *3*(11), 113604. https://doi.org/10.1103/physrevmaterials.3.113604

Badding, J., Hemley, R., & Mao, H. (1991). High-pressure chemistry of hydrogen in metals: In situ study of iron hydride. *Science*, *253*(5018), 421–424. https://doi.org/10.1126/science.253.5018.421

Badro, J., Brodholt, J. P., Piet, H., Siebert, J., & Ryerson, F. J. (2015). Core formation and core composition from coupled geochemical and geophysical constraints. *Proceedings of the National Academy of Sciences*, *112*(40), 12310–12314. https://doi.org/10.1073/pnas.1505672112

Badro, J., Fiquet, G., Guyot, F., Gregoryanz, E., Occelli, F., Antonangeli, D., & d'Astuto, M. (2007). Effect of light elements on the sound velocities in solid iron: Implications for the composition of Earth's core. *Earth and Planetary Science Letters*, *254*(1–2), 233–238. https://doi.org/10.1016/j.epsl.2006.11.025

Birch, F. (1947). Finite elastic strain of cubic crystals. *Physical Review*, *71*(11), 809–824. https://doi.org/10.1103/physrev.71.809

Birch, F. (1952). Elasticity and constitution of the Earth's interior. *Journal of Geophysical Research*, *57*(2), 227–286. https://doi.org/10.1029/jz057i002p00227

Cottaar, S., Heister, T., Rose, I., & Unterborn, C. (2014). BurnMan: A lower mantle mineral physics toolkit. *Geochemistry, Geophysics, Geosystems*, *15*(4), 1164–1179. https://doi.org/10.1002/2013gc005122

Dewaele, A., Loubeyre, P., Occelli, F., Mezouar, M., Dorogokupets, P. I., & Torrent, M. (2006). Quasihydrostatic equation of state of iron above 2 Mbar. *Physical Review Letters*, *97*(21), 215504. https://doi.org/10.1103/physrevlett.97.215504

Dorfman, S. M., Prakapenka, V. B., Meng, Y., & Duffy, T. S. (2012). Intercomparison of pressure standards (Au, Pt, Mo, MgO, NaCl and Ne) to 2.5 Mbar. *Journal of Geophysical Research*, *117*(B8). https://doi.org/10.1029/2012jb009292

Dziewonski, A. M., & Anderson, D. L. (1981). Preliminary reference Earth model. *Physics of the Earth and Planetary Interiors*, *25*(4), 297–356. https://doi.org/10.1016/0031-9201(81)90046-7

Edmund, E., Antonangeli, D., Decremps, F., Miozzi, F., Morard, G., Boulard, E., et al. (2019). Velocity-density systematics of Fe-5wt% Si: Constraints on Si content in the Earth's inner core. *Journal of Geophysical Research: Solid Earth*, *124*(4), 3436–3447. https://doi.org/10.1029/2018jb016904

Fei, Y., Murphy, C., Shibazaki, Y., Shahar, A., & Huang, H. (2016). Thermal equation of state of hcp-iron: Constraint on the density deficit of Earth's solid inner core. *Geophysical Research Letters*, *43*(13), 6837–6843. https://doi.org/10.1002/2016gl069456

Fei, Y., Ricolleau, A., Frank, M., Mibe, K., Shen, G., & Prakapenka, V. (2007). Toward an internally consistent pressure scale. *Proceedings of the National Academy of Sciences*, *104*(22), 9182–9186. https://doi.org/10.1073/pnas.0609013104

Finger, L., Hazen, R., Zou, G., Mao, H., & Bell, P. (1981). Structure and compression of crystalline argon and neon at high pressure and room temperature. *Applied Physics Letters*, *39*(11), 892–894. https://doi.org/10.1063/1.92597

Fischer, R. A., Campbell, A. J., Caracas, R., Reaman, D. M., Dera, P., & Prakapenka, V. B. (2012). Equation of state and phase diagram of Fe–16Si alloy as a candidate component of Earth's core. *Earth and Planetary Science Letters*, *357*, 268–276. https://doi.org/10.1016/j.epsl.2012.09.022

Fischer, R. A., Campbell, A. J., Caracas, R., Reaman, D. M., Heinz, D. L., Dera, P., & Prakapenka, V. B. (2014). Equations of state in the Fe-FeSi system at high pressures and temperatures. *Journal of Geophysical Research: Solid Earth*, *119*(4), 2810–2827. https://doi.org/10.1002/2013jb010898

Fischer, R. A., Campbell, A. J., Reaman, D. M., Miller, N. A., Heinz, D. L., Dera, P., & Prakapenka, V. B. (2013). Phase relations in the Fe–FeSi system at high pressures and temperatures. *Earth and Planetary Science Letters*, *373*, 54–64. https://doi.org/10.1016/j.epsl.2013.04.035

Fu, S., Chariton, S., Prakapenka, V. B., Chizmeshya, A., & Shim, S.-H. (2022). Stable hexagonal ternary alloy phase in Fe-Si-H at 28.6–42.2 GPa and 3000 K. *Physical Review B*, *105*(10), 104111. https://doi.org/10.1103/physrevb.105.104111

Fu, S., Chariton, S., Prakapenka, V. B., & Shim, S.-H. (2023). Core origin of seismic velocity anomalies at Earth's core–mantle boundary. *Nature*, *615*(7953), 1–6. https://doi.org/10.1038/s41586-023-05713-5

Fukai, Y. (1992). Some properties of the Fe-H system at high pressures and temperatures, and their implications for the Earth's core. *High Pressure Research: Application to Earth and Planetary Sciences*, 373–385.

He, Y., Sun, S., Kim, D. Y., Jang, B. G., Li, H., & Mao, H.-K. (2022). Superionic iron alloys and their seismic velocities in Earth's inner core. *Nature*, *602*(7896), 258–262. https://doi.org/10.1038/s41586-021-04361-x

Hirao, N., Ohtani, E., Kondo, T., & Kikegawa, T. (2004). Equation of state of iron–silicon alloys to megabar pressure. *Physics and Chemistry of Minerals*, *31*(6), 329–336. https://doi.org/10.1007/s00269-004-0387-x

Hirose, K., Wood, B., & Vocadlo, L. (2021). Light elements in the Earth's core. *Nature Reviews Earth & Environment*, *2*(9), 1–14. https://doi.org/10.1038/s43017-021-00203-6

Holland, T. J. B., & Redfern, S. A. T. (1997). Unit cell refinement from powder diffraction data: The use of regression diagnostics. *Mineralogical Magazine*, *61*(404), 65–77. https://doi.org/10.1180/minmag.1997.061.404.07

Huang, H., Fan, L., Liu, X., Xu, F., Wu, Y., Yang, G., et al. (2022). Inner core composition paradox revealed by sound velocities of Fe and Fe-Si alloy. *Nature Communications*, *13*(1), 1–9. https://doi.org/10.1038/s41467-022-28255-2

Huang, H., Leng, C., Wang, Q., Young, G., Liu, X., Wu, Y., et al. (2019). Equation of state for shocked Fe-8.6 wt% Si up to 240 GPa and 4,670 K. *Journal of Geophysical Research: Solid Earth*, *124*(8), 8300–8312. https://doi.org/10.1029/2019jb017983

Jackson, I., & Rigden, S. M. (1996). Analysis of PVT data: Constraints on the thermoelastic properties of high-pressure minerals. *Physics of the Earth and Planetary Interiors*, *96*(2–3), 85–112. https://doi.org/10.1016/0031-9201(96)03143-3

Jacobs, J. (1953). The Earth's inner core. *Nature*, *172*(4372), 297–298. https://doi.org/10.1038/172297a0

Jephcoat, A., & Olson, P. (1987). Is the inner core of the Earth pure iron? *Nature*, *325*(6102), 332–335. https://doi.org/10.1038/325332a0

Ji, C., Goncharov, A. F., Shukla, V., Jena, N. K., Popov, D., Li, B., et al. (2017). Stability of $Ar(H_2)_2$ to 358 GPa. *Proceedings of the National Academy of Sciences*, *114*(14), 3596–3600. https://doi.org/10.1073/pnas.1700049114

Loubeyre, P., Letoullec, R., & Pinceaux, J.-P. (1994). Compression of $Ar(H_2)_2$ up to 175 GPa: A new path for the dissociation of molecular hydrogen? *Physical Review Letters*, *72*(9), 1360–1363. https://doi.org/10.1103/physrevlett.72.1360

Martorell, B., Wood, I. G., Brodholt, J., & Vo˘cadlo, L. (2016). The elastic properties of hcp-$Fe_{1-x}Si_x$ at Earth's inner-core conditions. *Earth and Planetary Science Letters*, *451*, 89–96. https://doi.org/10.1016/j.epsl.2016.07.018

McDonough, W. F., & Sun, S.-S. (1995). The composition of the Earth. *Chemical Geology*, *120*(3–4), 223–253. https://doi.org/10.1016/0009-2541(94)00140-4

Miozzi, F., Matas, J., Guignot, N., Badro, J., Siebert, J., & Fiquet, G. (2020). A new reference for the thermal equation of state of iron. *Minerals*, *10*(2), 100. https://doi.org/10.3390/min10020100

Morrison, R. A., Jackson, J. M., Sturhahn, W., Zhao, J., & Toellner, T. S. (2019). High pressure thermoelasticity and sound velocities of Fe-Ni-Si alloys. *Physics of the Earth and Planetary Interiors*, *294*, 106268. https://doi.org/10.1016/j.pepi.2019.05.011

Pepin, C. M., Dewaele, A., Geneste, G., Loubeyre, P., & Mezouar, M. (2014). New iron hydrides under high pressure. *Physical Review Letters*, *113*(26), 265504. https://doi.org/10.1103/physrevlett.113.265504

Pepin, C. M., Geneste, G., Dewaele, A., Mezouar, M., & Loubeyre, P. (2017). Synthesis of FeH_5: A layered structure with atomic hydrogen slabs. *Science*, *357*(6349), 382–385. https://doi.org/10.1126/science.aan0961

Prescher, C., & Prakapenka, V. B. (2015). DIOPTAS: A program for reduction of two-dimensional X-ray diffraction data and data exploration. *High Pressure Research*, *35*(3), 223–230. https://doi.org/10.1080/08957959.2015.1059835

Sakai, T., Takahashi, S., Nishitani, N., Mashino, I., Ohtani, E., & Hirao, N. (2014). Equation of state of pure iron and $Fe_{0.9}Ni_{0.1}$ alloy up to 3 Mbar. *Physics of the Earth and Planetary Interiors*, *228*, 114–126. https://doi.org/10.1016/j.pepi.2013.12.010

Shen, G., Wang, Y., Dewaele, A., Wu, C., Fratanduono, D. E., Eggert, J., et al. (2020). Toward an international practical pressure scale: A proposal for an IPPS ruby gauge (IPPS-Ruby2020). *High Pressure Research*, *40*(3), 299–314. https://doi.org/10.1080/08957959.2020.1791107

Shim, S.-H. (2017). *PeakPo—A Python software for X-ray diffraction analysis at high pressure and high temperature*. Zenodo.

Shim, S.-H., & Duffy, T. S. (2000). Constraints on the *P-V-T* equation of state of $MgSiO_3$ perovskite. *American Mineralogist*, *85*(2), 354–363. https://doi.org/10.2138/am-2000-2-314

Singh, A. K., Balasingh, C., Mao, H.-K., Hemley, R. J., & Shu, J. (1998). Analysis of lattice strains measured under nonhydrostatic pressure. *Journal of Applied Physics*, *83*(12), 7567–7575. https://doi.org/10.1063/1.367872

Stixrude, L., & Lithgow-Bertelloni, C. (2005). Thermodynamics of mantle minerals—I. Physical properties. *Geophysical Journal International*, *162*(2), 610–632. https://doi.org/10.1111/j.1365-246x.2005.02642.x

Tagawa, S., Helffrich, G., Hirose, K., & Ohishi, Y. (2022). High-pressure melting curve of FeH: Implications for eutectic melting between fe and non-magnetic FeH. *Journal of Geophysical Research: Solid Earth*, *127*(6), e2022JB024365. https://doi.org/10.1029/2022jb024365

Tagawa, S., Ohta, K., Hirose, K., Kato, C., & Ohishi, Y. (2016). Compression of Fe–Si–H alloys to core pressures. *Geophysical Research Letters*, *43*(8), 3686–3692. https://doi.org/10.1002/2016gl068848

Tagawa, S., Sakamoto, N., Hirose, K., Yokoo, S., Hernlund, J., Ohishi, Y., & Yurimoto, H. (2021). Experimental evidence for hydrogen incorporation into Earth's core. *Nature Communications*, *12*(1), 1–8. https://doi.org/10.1038/s41467-021-22035-0

Takemura, K., & Dewaele, A. (2008). Isothermal equation of state for gold with a He-pressure medium. *Physical Review B*, *78*(10), 104119. https://doi.org/10.1103/physrevb.78.104119

Tateno, S., Kuwayama, Y., Hirose, K., & Ohishi, Y. (2015). The structure of Fe–Si alloy in Earth's inner core. *Earth and Planetary Science Letters*, *418*, 11–19. https://doi.org/10.1016/j.epsl.2015.02.008

Vocadlo, L., Alf`e, D., Gillan, M., Wood, I., Brodholt, J., & Price, G. D. (2003). Possible thermal and chemical stabilization of body-centred-cubic iron in the Earth's core. *Nature*, *424*(6948), 536–539. https://doi.org/10.1038/nature01829

Wang, W., Li, Y., Brodholt, J. P., Vo˘cadlo, L., Walter, M. J., & Wu, Z. (2021). Strong shear softening induced by superionic hydrogen in Earth's inner core. *Earth and Planetary Science Letters*, *568*, 117014. https://doi.org/10.1016/j.epsl.2021.117014

Ye, Y., Shim, S.-H., Prakapenka, V., & Meng, Y. (2018). Equation of state of solid ne inter-calibrated with the MgO, Au, Pt, NaCl-B2, and ruby pressure scales up to 130 GPa. *High Pressure Research*, *38*(4), 377–395. https://doi.org/10.1080/08957959.2018.1493477